STUDY ON THE EXPLOSION SUPPRESSION PERFORMANCE OF METHANE–AIR MIXTURES BASED ON $NH_4H_2PO_4$-MODIFIED DRY WATER GEL

Hao SUN[1,2], Guoxun JING[1,*], Chuang LIU[1,*], and Hailin JIA[1]

[1] College of Safety Science and Engineering, Henan Polytechnic University, Jiaozuo, China

[2] School of Intelligent Construction and Civil Engineering, Luoyang Institute of Science and Technology, Luoyang, China

[*] Corresponding author; E-mail: gxjing@hpu.edu.cn, liuchuang0714@126.com

As a vital energy source, methane poses significant explosion risks that threaten industrial safety. To address the limitations of conventional methane explosion suppressants, a modified dry water gel ($NH_4H_2PO_4$–SCDW) was prepared by incorporating 5 wt% $NH_4H_2PO_4$, 0.1 wt% sodium alginate (SA), and 0.05 wt% calcium lactate (CL). The physical properties and explosion suppression performance of the composite were systematically evaluated. Experimental results showed that $NH_4H_2PO_4$–SCDW exhibited not only excellent structural stability and water retention capability, but also rapid water release under high-temperature conditions, thereby effectively suppressing explosions. In pipeline explosion tests, $NH_4H_2PO_4$–SCDW exhibited significantly better suppression performance than conventional dry water (DW), with the peak overpressure at pressure sensor 1# reduced by approximately 16.95% on average, and the flame propagation distance shortened by 24.13% at a spray dosage of 0.48 g. Mechanism analysis revealed that $NH_4H_2PO_4$–SCDW suppresses methane combustion through the synergistic effects of physical and chemical inhibition, effectively interrupting the combustion chain reaction. This study provides theoretical support and experimental evidence for the development of high-efficiency and environmentally friendly fire and explosion suppressants.

Keywords: modified dry water gel ; methane explosion; synergistic suppression; suppression mechanism

1. Introduction

Methane (CH_4), as a vital energy resource, poses significant explosion risks in coal mining, petroleum extraction, and natural gas operations, seriously endangering human life and property safety [1, 2]. Consequently, the development of efficient methane explosion suppressants has become a critical focus in the field of disaster prevention and mitigation. Given that methane explosions involve complex physicochemical reaction processes [3, 4], effective prevention requires a deep understanding of the explosion mechanisms and characteristics of methane. Current suppression strategies primarily include powder suppression, water mist suppression, and inert gas suppression [5-8]. Although each method offers distinct advantages, they also present certain limitations [9]. Among them, powder suppressants have gained increasing attention due to their ease of storage and transportation. However, single-

component powders often exhibit limited suppression performance. Therefore, the development of composite suppressants—enhancing suppression effects through the synergistic action of multiple components—has become a key research trend.

As a novel composite material, DW contains up to 90% water and exhibits excellent fluidity and dispersibility [10], combining the advantages of both powder and water mist suppressants. In recent years, it has made remarkable progress in the fields of fire and explosion suppression. Existing studies have shown that DW can effectively lower flame temperature, delay flame propagation, absorb heat, and form a cooling barrier in the flame region, thereby significantly inhibiting explosions [11-13]. However, due to its unique core-shell structure, DW suffers from poor structural stability and is difficult to store. To enhance its performance, researchers have applied various modifications, such as incorporating different chemical additives or gel agents to improve its stability and suppression effectiveness [10, 11, 14]. Nevertheless, the structural stability and water retention capability of gels may also limit their explosion suppression performance. Studies have shown that the gel agent SA and the cross-linker CL can form a gel structure through cross-linking at low temperatures, which can be disrupted above 100 °C, enabling rapid water release [15, 16].

$NH_4H_2PO_4$, an environmentally friendly and non-toxic inorganic salt, has demonstrated excellent performance in fire and explosion suppression. Upon heating, $NH_4H_2PO_4$ decomposes and releases steam and ammonia, both of which can effectively suppress flame propagation and reduce the intensity and temperature of combustion [17, 18]. The combination of $NH_4H_2PO_4$ and DW not only leverages the superior cooling and suppression performance of DW gel but also provides additional chemical suppression effects through the decomposition products of $NH_4H_2PO_4$, thereby significantly improving the suppression of methane–air mixture explosions. To enhance the explosion suppression capability of DW and overcome its poor storage stability and low structural strength, this study prepared $NH_4H_2PO_4$–SCDW by incorporating SA, CL, and $NH_4H_2PO_4$ as gel and chemical additives. Its physical properties were characterized, and methane–air explosion suppression experiments were conducted using a custom-built pipeline system. Furthermore, suppression mechanisms of $NH_4H_2PO_4$–SCDW were analyzed through simulations. The findings of this study provide theoretical and experimental support for the development of efficient and environmentally friendly fire and explosion suppressants.

2. Experiments

2.1. Experimental Materials

Hydrophobic nano-silica (Degussa AERDSIL R812S) with an average particle size of 7 nm was used, which was prepared from AEROSIL 300 via treatment with HMDS (hexamethyldisilazane). Deionized water was prepared in-house. The modifier used was $NH_4H_2PO_4$, the gelator was SA, and the crosslinking agent was CL. Detailed information on the chemical reagents used in the experiments is provided in Table 1.

Enhancement of the structural stability and water retention of DW was achieved by employing natural linear polysaccharide SA as the gelator. The gelation process relies on the ionic cross-linking between SA molecular chains and divalent cations (e.g., Ca^{2+}) [19, 20]. The concentration of Ca^{2+} must be carefully controlled; if it is too low, insufficient cross-linking may occur, whereas excessively high concentrations could induce precipitation, thereby impeding the successful formation of DW. CL, when

dissolved in water, releases Ca^{2+} gradually, which facilitates the progressive gelation of the SA solution and provides a sufficient reaction time for DW formation.

Table 1. Materials Used in the Experiment

Material Name	Chemical Formula	Manufacturer	Purity
Hydrophobic Silica	SiO_2	Degussa AEROSIL	GR Superior Reagent
Deionized Water	H_2O	Laboratory-made	LR Laboratory Reagent
Ammonium dihydrogen phosphate	$NH_4H_2PO_4$	Sinopharm Chemical Reagent Co., Ltd.	AR Analytical Reagent
Sodium Alginate	SA	Sinopharm Chemical Reagent Co., Ltd.	CP Chemically Pure
L-Calcium Lactate	CL	Shanghai Aladdin Biochemical Technology Co., Ltd.	USP United States Pharmacopeia

Figure 1. Preparation process and mechanism of DW

Prior to the experiments, solutions of SA (base solution), $NH_4H_2PO_4$, and the CL cross-linker were prepared at predetermined concentrations and stored at 5°C for later use. During preparation, a 100 g mixed solution was formulated with 5 wt% $NH_4H_2PO_4$, 0.1 wt% SA, and 0.05 wt% CL. $NH_4H_2PO_4$-SCDW (or DW) was then prepared by mixing hydrophobic silica with the solution (or deionized water) at a mass ratio of 9:100. The detailed preparation process is illustrated in Figure 1. The mixing process utilized a JFS-550 disperser (550 W; speed range: 0–8000 r/min) produced by Hangzhou Qiwei Instrument Co., Ltd., which was equipped with custom composite blades designed to generate strong turbulence and high shear forces. The stirring speed was set at 5000 r/min and maintained for 4 minutes [21, 22].

2.2. Explosion Suppression Experiments

2.2.1 Experimental Equipment

A transparent square-pipe experimental system was constructed. This system primarily consists of the explosion tube, gas mixing unit, powder injection module, ignition system, pressure acquisition setup, high-speed imaging, and a synchronization control system, as illustrated in Figure 2. The explosion tube is composed of two sections of polymethyl methacrylate tubing (with a square cross-section of 80 mm × 80 mm): one end-sealed explosion chamber (with a length of 250 mm) and one open-ended flame propagation channel (with a length of 1000 mm). These are separated by a PVC film and

connected via a flange. The tube walls are 20 mm thick and withstand pressures up to 2 MPa. Sensor mounting ports are integrated along the pipe wall. The gas mixing module utilizes a methane cylinder, an air compressor, and a mass flow controller (ALICAT, USA) to prepare a methane–air mixture with a volume concentration of 9.0%. The powder injection system, installed at the central bottom of the explosion tube, consists of a powder reservoir, high-pressure gas chamber, and solenoid valve, enabling uniform dispersion of DW powder into the chamber. A 6 kV high-energy igniter serves as the ignition source. Pressure data are collected using four MD-HF pressure sensors, a National Instruments (NI) acquisition module, and a data card, with a sampling rate of 80 kS/s. A high-speed camera records explosion dynamics at 1000 frames per second. The explosion experiments were conducted under ambient temperature and pressure conditions. System-wide synchronization of initiation and shutdown is precisely managed using Omron automation equipment, ensuring coordinated operation across all subsystems.

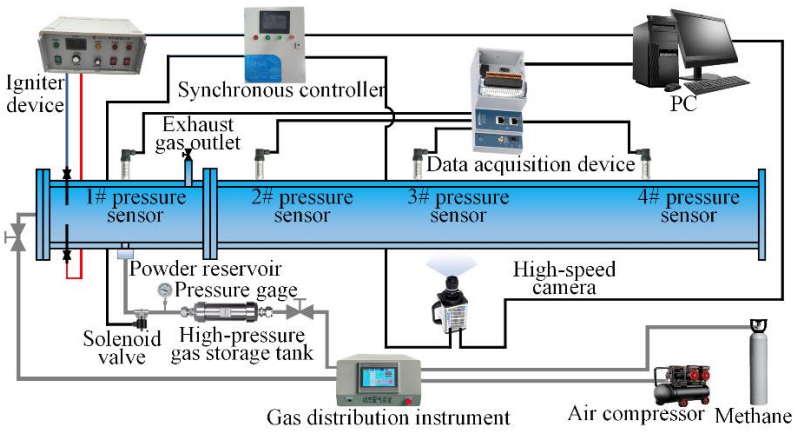

Figure 2. Experimental equipment

2.2.2 Experimental methodology

The experimental setup was assembled and calibrated according to the schematic shown in Figure 2. To ensure the accuracy of the methane–air premixed gas concentration, the explosion chamber was first purged with five times its volume of a 9.0% methane–air mixture. Subsequently, the same mixture was introduced into the high-pressure reservoir to reach the required pressure. Once gas filling was completed, the data acquisition system, high-speed camera, and solenoid valve for powder injection were activated simultaneously. After 150 ms, the solenoid valve was closed, and ignition was initiated using a 6 kV igniter for a duration of 100 ms. All systems were shut down 2 seconds after ignition. To ensure the reliability of the experimental data, each test condition was repeated at least three times. The average of three valid trials was taken as the final result.

3. Results and Discussion

3.1. Material Characterization

3.1.1 Structure and Morphology

Figure 3 presents the microscopic morphology of DW observed using a field emission scanning electron microscope (Quanta FEG 250). The image reveals that the nano-silica particles interlock to

encapsulate water, forming a porous core–shell structure. However, due to the lack of a supporting framework, DW exhibits several drawbacks, including high volatility, poor storage stability, low structural strength, and susceptibility to damage. Figure 4 illustrates the particle size distributions of DW and 5 wt% $NH_4H_2PO_4$-SCDW powders, measured using a Mastersizer 2000. The D(0.5) values of DW and 5 wt% $NH_4H_2PO_4$-SCDW are 141.76 μm and 110.49 μm, respectively, indicating that the addition of $NH_4H_2PO_4$, SA, and CL reduces the average particle size. Moreover, the D[3,2] and D[4,3] values of DW are both larger than those of $NH_4H_2PO_4$-SCDW, suggesting that the modified powder exhibits smaller and more uniform particle sizes. Additionally, powders with 10 wt% and 15 wt% $NH_4H_2PO_4$-SCDW were also prepared. However, measurements showed a significant presence of large particles exceeding 1000 μm in diameter. To eliminate the influence of particle size on the explosion suppression performance of DW, only DW and 5 wt% $NH_4H_2PO_4$-SCDW were selected for subsequent explosion suppression experiments.

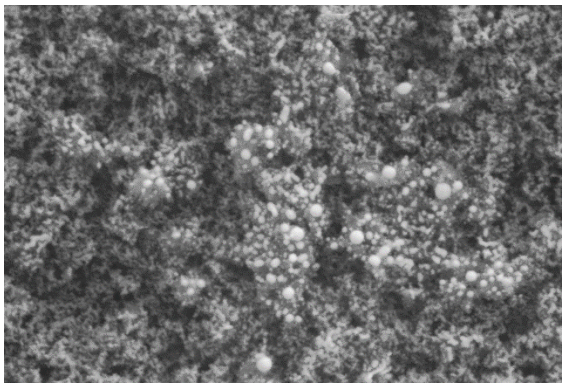

Figure 3. Microscopic morphology of DW powder

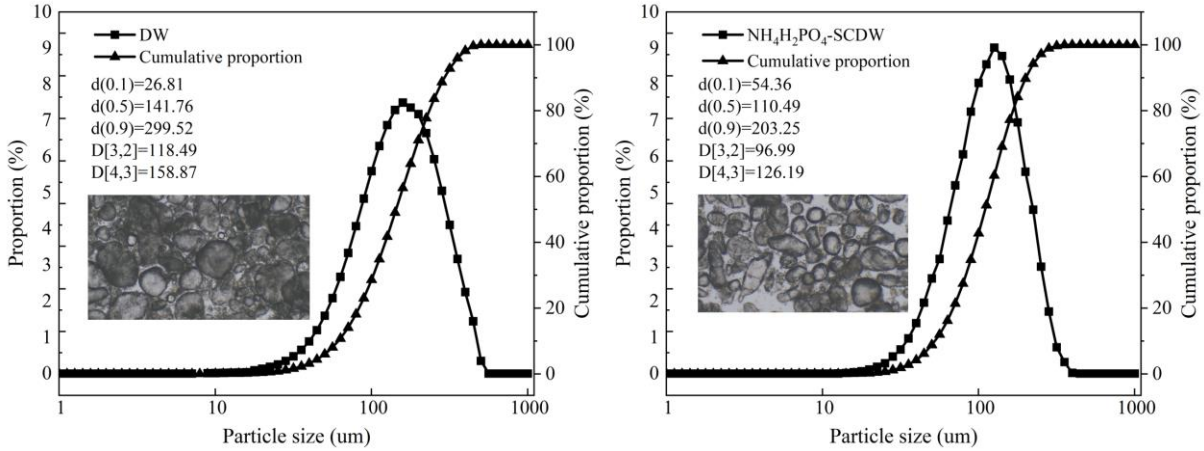

Figure 4. Particle size distribution of two types of DW

3.1.2 Mechanical Stability

A total of 0.5 g of DW and $NH_4H_2PO_4$-SCDW powders were evenly spread in a flat glass container and covered with a circular transparent glass plate (10 cm in diameter). By adjusting the weights placed on the cover, the applied pressure was set to 10 Pa, 50 Pa, 100 Pa, and 500 Pa, respectively, and maintained for 2 minutes. The damage states of the powder particles were observed under low magnification (0.5×) using a Nikon SMZ 745T stereomicroscope. ImageJ software was used

to analyze the proportion of damaged particles (only particles with diameters exceeding 100 μm were considered, for each image, 100 particles were analyzed, and the average value was obtained from three repetitions for each condition). The statistical results are presented in Figure 5. As shown in the figure, the damage ratio of both powders increases with rising pressure. At 500 Pa, the damage ratios for DW and $NH_4H_2PO_4$-SCDW were 77.33% and 27.17%, respectively. These results demonstrate that the $NH_4H_2PO_4$-SCDW powder possesses significantly higher structural stability compared to unmodified DW.

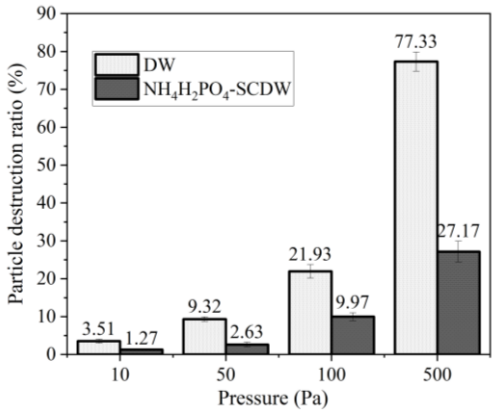

Figure 5. Damage behavior of two types of DW powder under compression

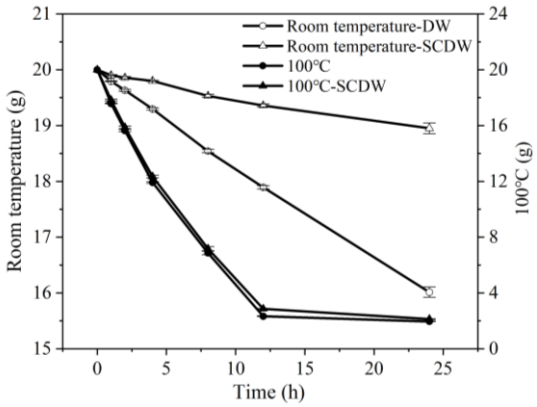

Figure 6. Water retention performance test of two DW powders

3.1.3 Mechanical Stability

Twenty grams of DW and $NH_4H_2PO_4$-SCDW powders were placed in an evaporating dish with a diameter of 100 mm, ensuring the surface of the powders remained even. The samples were placed in a temperature-controlled chamber at room temperature and 100°C for 24 hours. The remaining mass of the powders was recorded at 1, 2, 4, 8, 12, and 24 hours, as shown in Figure 6. At room temperature, the weight loss curves of both powders showed a linear distribution. After 24 hours, the water loss rates for DW and $NH_4H_2PO_4$-SCDW were 19.95% and 5.25%, respectively, indicating that the modified powder had a significantly lower water loss rate. At 100°C, both curves remained linear for the first 12 hours, after which the mass of the powders stabilized. This can be attributed to the degradation of the crosslinking structure of SA and CL in the high-temperature environment [15, 16], which resulted in a decreased water retention capacity and caused both powders to exhibit similar dehydration patterns beyond this point. In conclusion, this modified powder demonstrates excellent water retention at room temperature, while at high temperatures, it can rapidly release moisture, thus contributing to effective explosion suppression.

3.2. Inhibitory Effects of DW on Methane-Air Explosions

3.2.1 Overpressure Analysis with Inhibitors

Figure 7 shows the peak overpressure values of explosion shock waves measured by Sensors #1–#4 for DW and $NH_4H_2PO_4$-SCDW powders under different spraying masses (0.08 g, 0.16 g, 0.32 g, 0.48 g, 0.64 g, and 0.80 g). The results indicate that as the spraying mass increases, the maximum explosion pressure decreases rapidly within the range of 0.08–0.32 g, with average pressure reductions of 67.85% and 73.68% for DW and $NH_4H_2PO_4$-SCDW, respectively. Beyond 0.32 g, the pressure decline slows.

Notably, a pressure peak is observed at 0.64 g for Sensor #1, attributed to the accumulation of pressure caused by the formation of an insulating layer on the PVC membrane surface due to excessive DW particles. This layer delays the rupture of the membrane, but further increases in spraying mass eventually reduce the pressure generated in the explosion chamber. $NH_4H_2PO_4$–SCDW exhibits superior suppression efficacy compared to DW, reducing average pressures at Sensors #1–#4 by 16.95%, 5.95%, 37.20%, and 41.34%, respectively.

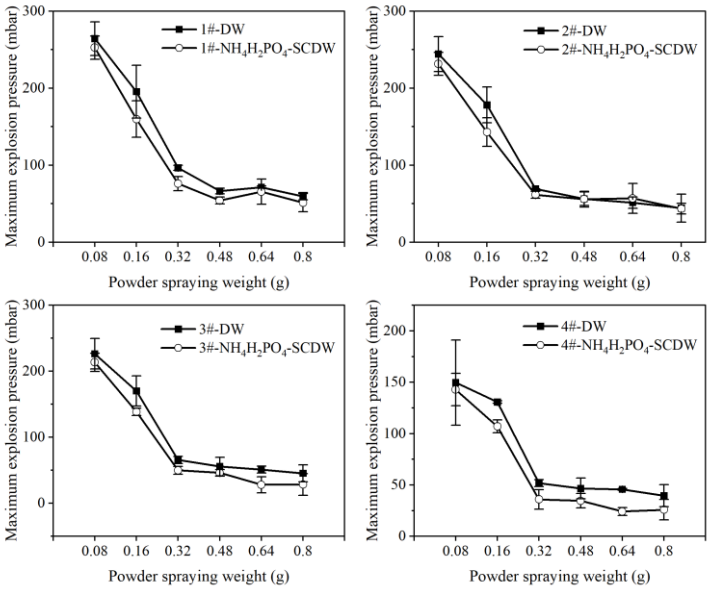

Figure 7. Effect of Two DW Powders on the Maximum Pressure of Methane-Air Explosions

3.2.2 Influence on Flame Structure

Figure 8 illustrates the flame propagation behavior during the explosion of a 9.0% methane–air premixed gas under four different conditions: without inhibitor, and with 0.08 g, 0.48 g, and 0.80 g of DW powder. In the absence of an inhibitor, the flame fully propagates throughout the entire tube, with a predominant yellow color and the appearance of pale blue flames around the flame front during the early stage of the explosion. After introducing DW powder as a suppressant, the flame does not reach the full length of the tube in any of the three mass conditions. Flame propagation velocity is significantly reduced, and the flame remains visible at 108 ms in all cases—indicating longer flame duration compared to the uninhibited condition. When 0.08 g of DW is applied, the flame appears bright yellow with the blue flame disappearing, which is attributed to water evaporation from the DW that lowers flame temperature. The flame reaches up to 91.5% of the tube length. At 0.48 g dosage, the flame turns dim yellow and extends to 63.2% of the tube. At 0.80 g, the dim yellow flame is successfully confined within the explosion chamber. In addition, under the four aforementioned conditions, the average flame propagation speeds from ignition to the farthest point in the tube were 66.67 m/s, 54.91 m/s, 25.28 m/s, and 7.50 m/s, respectively. Therefore, as the sprayed mass of DW increases, the explosion of the gas mixture can be significantly suppressed.

Figure 9 presents flame propagation behavior with 0.08 g, 0.48 g, and 0.80 g of $NH_4H_2PO_4$–SCDW powder. In all three cases, the flame appears dim yellow and does not fill the entire tube. Except for the 0.80 g case, the flame is extinguished before 108 ms. At 0.08 g, discontinuous flame propagation is observed, and a whitish-yellow flame appears at the front, indicating that $NH_4H_2PO_4$–SCDW effectively disrupts sustained combustion. The flame reaches 80.7% of the tube length. At 0.48 g, similar

discontinuities occur, and the flame extends only to 46.2% of the tube. With 0.80 g, the flame is contained within the explosion chamber. Under the three spraying mass conditions, the average flame propagation speeds were 34.59 m/s, 19.81 m/s, and 6.01 m/s, respectively, which represent reductions of 37.01%, 24.13%, and 19.87% compared to DW. In summary, $NH_4H_2PO_4$–SCDW outperforms DW powder in reducing flame propagation distance, disrupting flame continuity, and shortening flame duration.

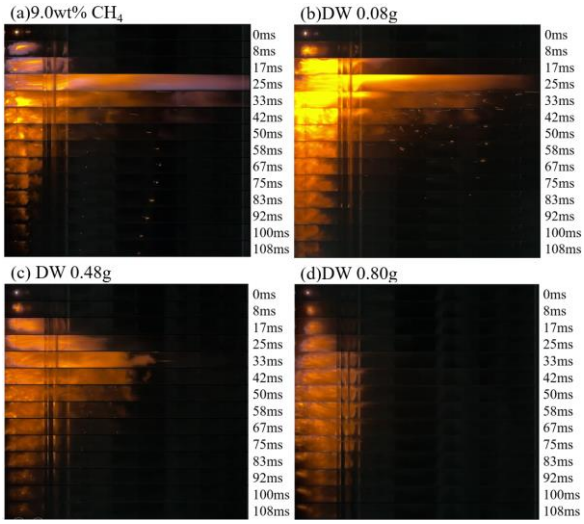

Figure 8. Effect of Different DW Spraying Concentrations on Flame Structure

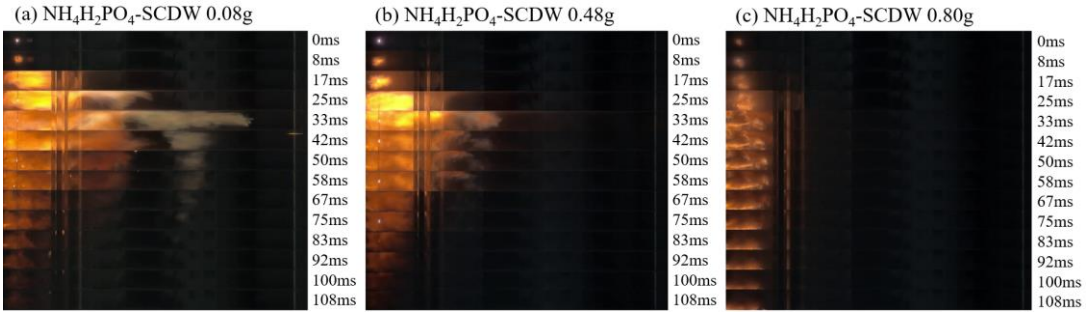

Figure 9. Effect of Different $NH_4H_2PO_4$-SCDW Spraying Concentrations on Flame Structure

3.3. Explosion Suppression Mechanism

3.3.1 Physical Suppression Mechanism

The thermal stability of DW and 5 wt% $NH_4H_2PO_4$–SCDW was evaluated using a NETZSCH STA449F3 simultaneous thermal analyzer at a heating rate of 10 °C/min over the temperature range of 25–800 °C. Figure 10 presents the thermogravimetry (TG), differential scanning calorimetry (DSC), and derivative thermogravimetry (DTG) curves for both powders. The TG curves show significant mass loss (over 90%) between 25 °C and 150 °C, primarily due to water evaporation. Above 150 °C, the mass remains relatively stable, indicating the thermal decomposition of SA and $NH_4H_2PO_4$. At 800 °C, the residual mass is 8.95% for DW and 9.13% for $NH_4H_2PO_4$–SCDW, primarily composed of SiO_2 and decomposition products. The DSC curves indicate total heat absorption values of 1537.61 J/g for DW and 1346.73 J/g for $NH_4H_2PO_4$–SCDW, demonstrating that both materials have low decomposition temperatures and high heat absorption capacities. DW exhibits greater heat absorption, attributed to its higher water content.

During explosion, water in both DW and $NH_4H_2PO_4$–SCDW absorbs heat and vaporizes into steam. Concurrently, $NH_4H_2PO_4$ decomposes, releasing NH_3, which lowers the reaction temperature and reduces oxygen concentration. Additionally, the powders—uniformly dispersed in the explosion chamber—impede thermal radiation and absorb part of the explosive energy through inter-particle collisions, thereby achieving physical suppression.

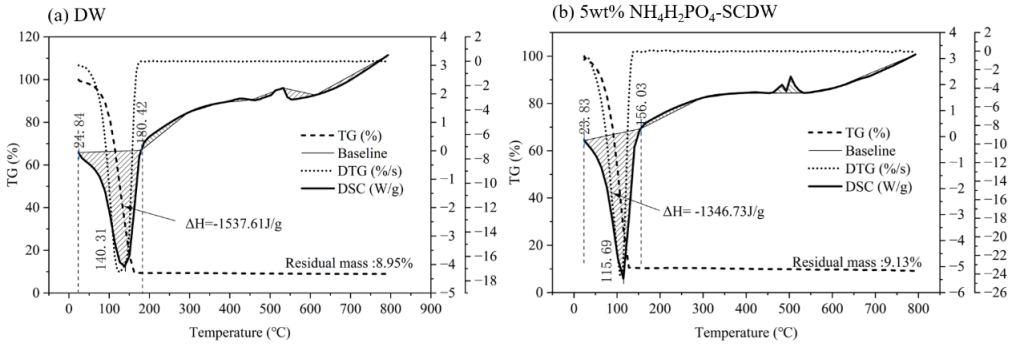

Figure 10. TG, DSC, and DTG Curves of DW and 5wt% $NH_4H_2PO_4$-SCDW

3.3.2 Chemical Suppression Mechanism

To analyze the pyrolysis characteristics of $NH_4H_2PO_4$–SCDW powder during methane–air explosions and the generation mechanism of active species, HSC Chemistry 6 software was used to simulate the equilibrium products and their quantities at different temperatures, as shown in Figure 11. Between 25 °C and 484 °C, $NH_4H_2PO_4$ decomposes to produce polyphosphoric acid (PPA), NH_3(g), and H_2O(g). From 484 °C to 1500 °C, PPA undergoes further thermal decomposition to generate inert oxide P_2O_5, with continued release of NH_3(g) and H_2O(g) during this stage [23]. Studies have shown that during its thermal decomposition, PPA consumes large quantities of active H and OH free radicals, thereby inhibiting combustion. Although the decomposition of $NH_4H_2PO_4$ and PPA produces significant amounts of NH_3(g), its low concentration among the equilibrium products suggests that it actively participates in the methane–air combustion process. NH_3(g) reacts with OH free radicals to form the final product H_2O(g), thereby interrupting the combustion chain reaction. Therefore, in the reaction kinetics of methane–air explosion suppression, $NH_4H_2PO_4$-modified DW exerts its effect primarily through the active species PPA and NH_3(g), which capture and consume flame free radicals, effectively terminating the chain reaction.

Based on the above analysis of the active species involved in flame inhibition, a numerical simulation was conducted using ANSYS CHEMKIN to further investigate the suppression mechanism of $NH_4H_2PO_4$, specifically focusing on the inhibitory effect of its decomposition product NH_3 on methane explosions.The simulation model adopts a zero-dimensional homogeneous reactor assumption, and the gas-phase chemical kinetics are based on the validated GRI-Mech 3.0 mechanism [22]. The model assumes that the DW particles are fully vaporized within the reaction zone, and surface kinetic effects on particle surfaces are neglected [24, 25].

Figure 12 presents the top 10 most sensitive reactions at the time of the maximum temperature gradient during methane–air combustion, with NH_3 (a decomposition product of $NH_4H_2PO_4$) acting as an inhibitor. A positive sensitivity coefficient indicates promotion of the combustion process, while a negative value indicates suppression. The magnitude reflects the strength of the effect, and sensitivity coefficients were normalized for comparison. The results show that, compared to the case without inhibitors, the sensitivity coefficients significantly decrease upon NH_3 addition, indicating a reduction

in reaction rates. In the absence of the inhibitor, the primary promoting reactions are R155 and R156, whereas the main inhibiting reactions are R53 and R158. After adding NH_3, the key promoting reactions shift to R32 and R155, and the major inhibiting reactions become R158 and R278. Studies have shown that reactions promoting combustion typically involve the generation of H and OH free radicals, while those that inhibit combustion involve their consumption [26]. Therefore, the effectiveness of an inhibitor can be evaluated by its ability to capture and consume H and OH free radicals [21]. With NH_3 present, reactions R277 and R288 consume H and OH free radicals, thereby suppressing combustion and significantly reducing the overall reaction rate.

Figure 13 shows the total generation rates of H and OH free radicals over time in the absence and presence of NH_3. The results align with the temperature sensitivity analysis: the addition of NH_3 markedly reduces the overall generation rates of H and OH free radicals, with decreases of 93.95% and 95.35%, respectively, indicating that NH_3 is highly effective in suppressing CH_4 combustion.

In summary, $NH_4H_2PO_4$–SCDW mitigates methane explosions through a combination of physical and chemical effects. Physically, TG-DSC analysis indicates that water evaporation absorbs heat, lowers oxygen concentration, and impedes thermal radiation and energy transfer via particle collisions. Chemically, HSC Chemistry and CHEMKIN simulations demonstrate that at elevated temperatures, $NH_4H_2PO_4$–SCDW decomposes to release PPA and NH_3, which capture H and OH free radicals, converting them into stable H_2O molecules. This process significantly reduces the overall reaction rate, effectively suppressing the explosion. Through both physical and chemical inhibition, the methane–air explosion was effectively controlled, as evidenced by the reduced peak explosion pressure, shortened flame propagation distance, and slower flame propagation velocity. Due to its chemical suppression effect, $NH_4H_2PO_4$–SCDW exhibited better inhibition performance than DW.

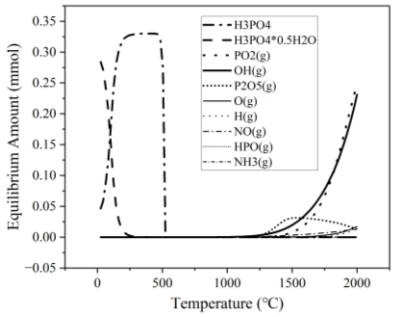

Figure 11. Equilibrium Products of Modified SCDW with Methane-Air Mixture

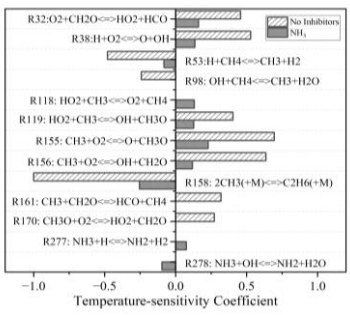

Figure 12. Temperature Sensitivity Coefficients of NH_3-Containing Methane-Air Combustion

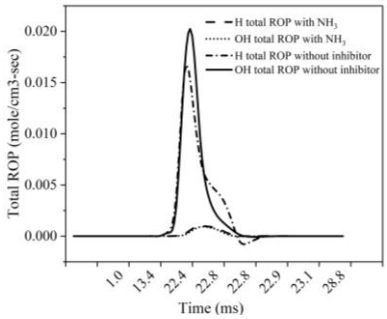

Figure 13 Total Rate of Production (ROP) of H and OH Free Radicals

4. Conclusion

This study systematically analyzed $NH_4H_2PO_4$–SCDW using both experimental and simulation approaches. The results demonstrate that the modified $NH_4H_2PO_4$–SCDW exhibits significantly improved mechanical stability, water retention, and explosion suppression performance compared to conventional DW. The main conclusions are as follows:

(1) $NH_4H_2PO_4$–SCDW exhibits excellent physical properties. Compared to DW, its mechanical stability is significantly enhanced, with a particle breakage rate of only 27.17% under 500 Pa pressure,

in contrast to 77.33% for DW, indicating a nearly threefold increase in compressive resistance. Its water retention at room temperature is also substantially improved, with a 24-hour water loss rate as low as 5.25%, compared to 19.95% for DW, thereby extending storage stability. In addition, its particle size distribution is more uniform, with a D(0.5) value of 110.49 μm, representing a 22.1% reduction compared to DW.

(2) In methane–air explosion experiments, the explosion suppression performance of $NH_4H_2PO_4$–SCDW was comprehensively superior to that of DW. The experimental results showed that with increasing spray dosage, both explosion overpressure and flame propagation velocity exhibited a stepwise decline. Notably, even at a moderate dosage (0.48 g), a significant reduction in explosion pressure and a marked shortening of flame propagation distance were achieved. Compared with DW, the modified material reduced the average explosion pressure by approximately 16.95% and shortened the flame propagation distance by about 24.13%.

(3) $NH_4H_2PO_4$–SCDW mitigates explosions through physical mechanisms—such as heat absorption via water evaporation, oxygen concentration reduction, energy dissipation through particle collisions, and thermal radiation shielding—and chemical mechanisms, including the thermal decomposition of $NH_4H_2PO_4$ into PPA and NH_3, which capture H and OH free radicals (reducing their generation rates by 93.95% and 95.35%, respectively), thereby interrupting the chain reaction.

Acknowledgment

This work was supported by the Joint Funds of the National Natural Science Foundation of China (Grant No. U1904210), the General Program of National Natural Science Foundation of China (Grant No. 52274185).

References

[1] Liu, Z.*, et al.*, Effect of high pressure on the performance of coalescing filter cartridges for the natural gas purification, *Process Safety and Environmental Protection*, *148* (2021), pp. 1077-1089

[2] Feng, L.*, et al.*, Gas production performance of underground coal gasification with continuously moving injection: Effect of direction and speed, *Fuel*, *347* (2023), pp.

[3] Cao, Y.*, et al.*, Influence of vent size and vent burst pressure on vented ethylene-air explosion: Experimental and numerical study, *Process Safety and Environmental Protection*, *170* (2023), pp. 297-309

[4] Zhang, C.*, et al.*, Flame propagation characteristics and surface functional groups changes of corn starch dust during the combustion process, *Powder Technology*, *430* (2023), pp.

[5] Zheng, L.*, et al.*, Effect of blockage ratios on the characteristics of methane/air explosion suppressed by BC powder, *Journal of Hazardous Materials*, *355* (2018), pp. 25-33

[6] Dounia, O.*, et al.*, Theoretical analysis and simulation of methane/air flame inhibition by sodium bicarbonate particles, *Combustion and Flame*, *193* (2018), pp. 313-326

[7] Qiu, D.*, et al.*, Explosion characteristics and suppression evaluation of hydrogen mixed with low-concentration aluminum powder, *International Journal of Hydrogen Energy*, *58* (2024), pp. 1552-1561

[8] Qiu, D.*, et al.*, Preparation of modified fly ash-based, core-shell inhibitor and its effect on suppression of Al-Mg alloy dust explosion, *Chemical Engineering Journal*, *468* (2023), pp.

[9] Qiu, D.*, et al.*, Application of microencapsulated fibrous carrier inhibitors in suppressing flake

aluminum dust explosion: Performance and mechanism, *Combustion and Flame*, *261* (2024), pp.
[10] Zou, Y.*, et al.*, Inspiration from a thermosensitive biomass gel: A novel method to improving the stability of core-shell "dry water" fire extinguishing agent, *Powder Technology*, *356* (2019), pp. 383-390
[11] Chen, X.*, et al.*, Renewable biomass gel reinforced core-shell dry water material as novel fire extinguishing agent, *Journal of Loss Prevention in the Process Industries*, *59* (2019), pp. 14-22
[12] Gao, J.*, et al.*, Investigation on the synergistic suppression effect of flame retardant-modified dry water on methane explosion, *Powder Technology*, *454* (2025), pp.
[13] Qiu, D.*, et al.*, Experimental exploration on the suppression of methane-air mixture explosions by bio-based modified gel dry water materials, *Thermal Science and Engineering Progress*, *60* (2025), pp.
[14] He, S.*, et al.*, Insight to hydrophobic SiO₂ encapsulated SiO₂ gel: Preparation and application in fire extinguishing, *Journal of Hazardous Materials*, *405* (2021), pp.
[15] Roopa, B.S., Bhattacharya, S., ALGINATE GELS: II. STABILITY AT DIFFERENT PROCESSING CONDITIONS, *Journal of Food Process Engineering*, *33* (2010), 3, pp. 466-480
[16] Andresen, I.-L., Smidsørod, O., Temperature dependence of the elastic properties of alginate gels, *Carbohydrate Research*, *58* (1977), 2, pp. 271-279
[17] Zhang, T.*, et al.*, Experimental research on combustible gas/air explosion inhibition by dry water, *International Journal of Hydrogen Energy*, *48* (2023), 93, pp. 36605-36620
[18] Liang, G.*, et al.*, Inhibition characteristics of coal dust explosion at the gasification atmosphere, *Advanced Powder Technology*, *32* (2021), 10, pp. 3725-3734
[19] Hou, Y.*, et al.*, Alginate-based aerogels with double catalytic activity sites and high mechanical strength, *Carbohydrate Polymers*, *245* (2020), pp.
[20] Liu, J., Xiao, C., Fire-retardant multilayer assembled on polyester fabric from water-soluble chitosan, sodium alginate and divalent metal ion, *International Journal of Biological Macromolecules*, *119* (2018), pp. 1083-1089
[21] Cai, C.*, et al.*, Suppressive effects of potassium salt modified dry water material on hydrogen/methane mixture explosion, *International Journal of Hydrogen Energy*, *79* (2024), pp. 537-550
[22] Wang, Q.*, et al.*, Gas explosion suppression performance of modified gel-type dry waters, *Powder Technology*, *420* (2023), pp.
[23] Liu, L.*, et al.*, Effect of powder inhibitors on ignition sensitivity evolution of wood-plastic mixed dust: Based on thermal decomposition behavior and deflagration residues, *Process Safety and Environmental Protection*, *160* (2022), pp. 265-273
[24] Wang, Y.*, et al.*, Inhibition Effect of KHCO3 and KH2PO4 on Ethylene Explosion, *Acs Omega*, (2023), pp.
[25] Zhou, J.*, et al.*, Flame suppression of 100 nm PMMA dust explosion by KHCO₃ with different particle size, *Process Safety and Environmental Protection*, *132* (2019), pp. 303-312
[26] Sun, Y.*, et al.*, Suppression of methane/air explosion by kaolinite-based multi-component inhibitor, *Powder Technology*, *343* (2019), pp. 279-286

Received: 19.04.2025.
Revised: 23.05.2025.
Accepted: 06.06.2025.